

A NEW FILTER FOR SPOT EXTRACTION IN N-DIMENSIONAL BIOLOGICAL IMAGING

Eric BIOT^{1,2}, Elizabeth CROWELL¹, Herman HÖFTE¹, Yves MAURIN²,
Samantha VERNHETTES¹ and Philippe ANDREY^{2,3}

¹Laboratoire de Biologie Cellulaire, Institut Jean-Pierre Bourgin, INRA, Versailles, France

²Analyse et Modélisation en Imagerie Biologique, Laboratoire de Neurobiologie de l'Olfaction
et de la Prise Alimentaire, INRA UMR 1197, Jouy-en-Josas, France

³Université Pierre et Marie Curie, Paris, France

ABSTRACT

In confocal cellular imaging, fluorescent markers are used to label target structures. These elements of interest frequently appear as spots within a noisy background. Several algorithms have been proposed to extract spots in such conditions. However, specific methods are required when other structures are also labelled. In this paper, a new spot extraction filter is proposed to discriminate between spots and other structures using the shape of the local spatial intensity distribution. Preliminary results in the analysis of the intra-cellular distribution of the KORRIGAN1 protein in plant cells are presented. Very low detection error rates are reported.

Index Terms— Confocal microscopy, cellular imaging, spot detection, spatial distribution.

1. INTRODUCTION

Plant cells are surrounded by a wall that plays a major role in organism growth and shape. The mechanisms regulating wall synthesis and expansion are still unknown. The KORRIGAN1 protein (KOR1) is an essential enzyme in wall elongation. It is principally located within an heterogeneous population of intra-cellular compartments and vesicles. Using confocal imaging in epidermal root cells of plants expressing KOR1 coupled to the green fluorescent protein (GFP), it has been shown that experimentally inhibiting wall synthesis produces a spatial redistribution of KOR1 towards the external cellular face [7]. This suggests a link between the regulation of wall synthesis and the intra-cellular distribution of some of the enzymes involved in this biochemical pathway.

However, the spatial analysis in [7] was based on the proportion of vesicles located above the upper limit of the vacuole. This does not provide a complete description of the GFP-KOR1 distribution. Moreover, the analysis was manually performed. It may thus have been biased by operator subjectivity. Lastly, manual processing is tedious and time consuming. It is unwieldy to repeat on large number of images

This work was supported by grant no. ANR-06-BLAN-0262-02 from the French Agence Nationale de la Recherche.

under various biological and experimental conditions. Hence, automated tools are required to perform large scale analyses of the spatial distributions of wall synthesis proteins.

In confocal microscopy images, GFP-KOR1 vesicles appear as bright spots. Several algorithms for spot detection in fluorescent imagery have been proposed in the past, including approaches based on mathematical morphology [5], wavelets [6], or Gaussian fit of intensity profiles [3]. Very good results can be obtained, in particular when prior knowledge, such as number of spots or absence of any other labelled structure, can be exploited [8, 5]. In our context, however, we are faced with several difficulties. First, the number of vesicles is unknown and highly variable. Second, the diameter of the vesicles is also variable and may vary with experimental conditions [7]. Third, other structures such as the membrane of the vacuole are also labelled. The presence of such structures must be explicitly taken into account into the spot extraction process to reach low error rates.

In this paper, a new filter for spot extraction is presented. It is specifically designed to discriminate between spots and other structures. We rely on the assumption that spots can be detected using the spatial isotropy of local intensities. We introduce an index to quantify isotropy from the spectrum of the local second-order moment matrix. The algorithm is described in Section 2. The method was applied to reexamine the GFP-KOR1 intra-cellular distribution. The first results, obtained in control conditions, are reported and briefly discussed in Section 3. Section 4 concludes the paper.

2. MATERIAL AND METHODS

2.1. Plant material and image acquisition

Arabidopsis plants expressing KOR1 fused to GFP [7] were grown in light at 20°C for 48 hours on strips of sterile nylon placed on media without sucrose as described in [4]. Seedlings were mounted in 0.8% low-melt agarose (Sigma) containing 50 μ M FM4-64 (Molecular Probes, Invitrogen) and visualised on a spectral Leica SP2 AOBs confocal microscope (Leica Microsystems). For each seedling, two

image stacks were acquired: GFP fluorescence was used to visualise KOR1 distribution; FM4-64 fluorescence was used to visualise cell boundaries. GFP was excited at 488 nm and fluorescence emission collected between 490 and 551 nm. Fluorescence emission of FM4-64 was collected between 645 and 833 nm. Z series of epidermal root cells (0.33 μm step interval, 256 \times 256 pixels of size 0.153 μm^2) were acquired using a 40X oil objective and a zoom factor of 9.57X.

2.2. Attenuation correction

It was generally observed that the recorded GFP signal intensity decreased with depth position in image stacks. Signal attenuation with depth is a common artefact in confocal microscopy imaging. It results both from photobleaching and from light absorption by the upper part of the sample. Signal attenuation has to be corrected prior to spot extraction to avoid any depth bias.

We propose here a simple attenuation correction that relies on the assumption that the image background should be stationary throughout an image stack. Accordingly, the correction aims at rectifying the background average intensity and standard-deviation. For each image of the stack, the background is estimated by applying a grey level morphological opening with a flat 7 \times 7 structuring element and its intensity average m and standard-deviation s are computed. The original image is then corrected according to:

$$I_{\text{corrected}} = m^* + s^* \times \frac{I_{\text{initial}} - m}{s} \quad (1)$$

where m^* and s^* are the background intensity average and standard-deviation of a reference slice. The upper slice of the stack was selected as reference since it was the less affected by the attenuation phenomenon.

2.3. Spot extraction

Images are first preprocessed to attenuate noise using a 3 \times 3 \times 3 average filter. The principle of the spot extraction filter described below is to detect positions with an isotropic local intensity distribution. However, vesicles are not the only structures producing such patterns. In particular, foldings of the vacuole membrane can produce domains of intense labelling that could be interpreted as very large spots. Hence, a white top-hat with a structuring element of size 7 \times 7 \times 7 and spherical intensity profile was applied to the noise-filtered images to eliminate such artefacts.

Following noise reduction and large blobs removal, two different kind of structures subsist in the images: vesicles and vacuole membranes. A new filter was designed to discriminate between them. Around a spot position, the intensity is expected to be distributed symmetrically in all directions. Conversely, it is expected to obey a planar distribution around a membrane position. Hence, spots correspond to positions

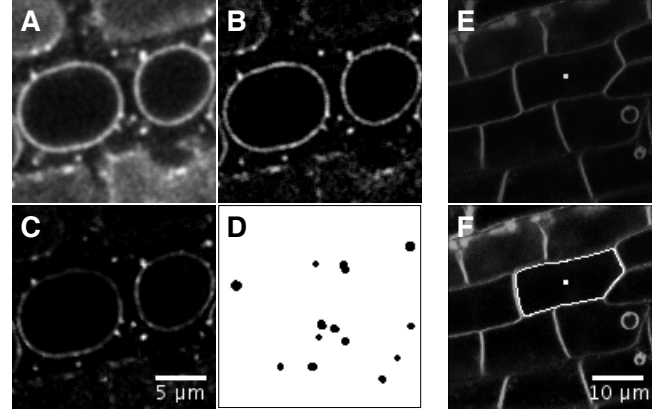


Fig. 1. Image processing: extraction of spots and cell boundaries. (A) Slice from a GFP stack after attenuation correction and noise reduction. (B) Top-hat filtering of A. (C) Isotropy filtering of B. (D) Thresholding of C. (E) Slice from a FM4-64 stack with a user-defined cell marker. (F) Final position of the active contour run from the cell marker. The dynamic ranges of B and C have been stretched to enhance readability.

where the local intensity distribution is isotropic. We propose to characterise isotropy based on the spectrum of the local second-order moments matrix M . In the 3D case, we have:

$$M = \begin{pmatrix} M_{xx} & M_{xy} & M_{xz} \\ M_{yx} & M_{yy} & M_{yz} \\ M_{zx} & M_{zy} & M_{zz} \end{pmatrix} \quad (2)$$

with

$$M_{xx} = \frac{\sum (x - \bar{x})^2 I(x, y, z)}{\sum I(x, y, z)} \quad (3)$$

$$M_{xy} = \frac{\sum (x - \bar{x})(y - \bar{y}) I(x, y, z)}{\sum I(x, y, z)} \quad (4)$$

and so forth, the sums running over the neighbourhood of the current position. The centroid of the neighbourhood is given by $\bar{x} = \frac{\sum x I(x, y, z)}{\sum I(x, y, z)}$ and similarly for the other two coordinates.

The eigenvalues $\{\lambda_i\}$ of M are the variances of the distribution along the principal axes of the neighbourhood. In an n -dimensional image, the ratio:

$$\frac{\lambda_i}{\sum_{j=1}^n \lambda_j} \quad (5)$$

is thus the proportion of the total dispersion that is observed along the i th principal direction. Under an ideal isotropic distribution, all such ratios are equal so that their product:

$$\prod_{i=1}^n \frac{\lambda_i}{\sum_{j=1}^n \lambda_j} = \frac{\det M}{(\text{tr} M)^n} \quad (6)$$

reaches its maximum value $(\frac{1}{n})^n$. Accordingly, we propose to quantify isotropy using the following index:

$$\text{isotropy index} = n \left[\frac{\det M}{(\text{tr} M)^n} \right]^{\frac{1}{n}} \quad (7)$$

which is the quantity of Equation 6 normalised within [0; 1].

Both spots and flat background regions yield high isotropy values. However, they differ in that spots also present high grey levels. The output of the filter is thus defined as a combination of isotropy and initial intensity. Since their magnitudes differ, the two quantities are combined through their product:

$$\text{Output image} = \text{isotropy index} \times \text{input image} \quad (8)$$

Spots are obtained by thresholding of the output image followed by connected component labelling. The filter has been designed for the three-dimensional case but can be applied to any n -dimensional image as well.

The algorithm has been implemented in C++ and integrated into the freely available Free-D reconstruction and modelling software [2]. The implementation is optimised by computing matrix M coefficients using moving sums $\sum f(x, y, z)$, $\sum x f(x, y, z)$, $\sum x^2 f(x, y, z)$, etc. However, special care is required to prevent arithmetic overflow and numerical instabilities when working on floating-point images. In particular, x , y and z must be expressed in the local coordinate frame centered around the current position.

2.4. Extraction of cell boundaries

Each image stack contained several cells. Analysing the intra-cellular distribution of GFP-KOR1 detected vesicles requires that they are assigned to their respective cells. It is thus necessary to determine cell boundaries. These were extracted from the FM4-64 channel images using an interactive procedure allowing cell selection. The user clicks in each cell to analyse, at any level in the stack. A circle centered on the specified position is then used to initialise an active contour algorithm that converges towards the cell boundary [1]. For each slice of the stack, the software automatically replicates the user-specified position and runs the active contour algorithm. If necessary, the resulting contour stack can be edited using Free-D tools. Surface meshes are generated from contours and displayed as opaque or transparent surfaces for 3D rendering.

2.5. Evaluation of spot extraction

To evaluate error rates, automatic spot extraction was compared to manual analysis. To this end, twenty cells were manually processed within Free-D. Using the mouse, each spot was recorded as a point. In parallel, the 20 test cells were processed using the spot extraction algorithm. Manually recorded positions contained within no automatically extracted spot counted as false negatives. Conversely, automatically detected spots containing no manually recorded position counted as false positives.

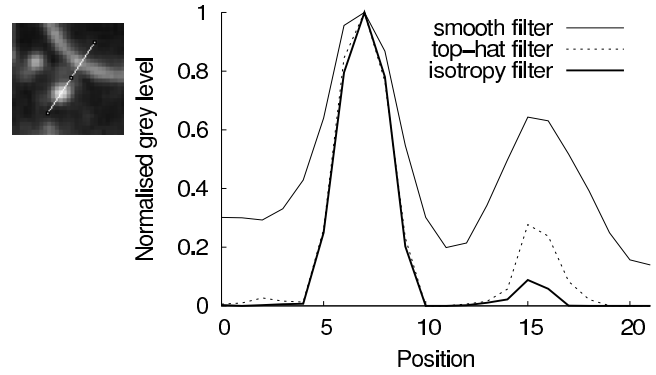


Fig. 2. Spot extraction: grey level profiles following attenuation correction and noise reduction, top-hat filtering, and isotropy filtering. Profiles were normalised at their maxima. The position of the profile is shown at top left.

2.6. Analysis of spot intra-cellular distribution

In order to conform to the manual analysis reported earlier [7], the distribution of GFP-KOR1 vesicles was analysed along the z -direction. Positions were normalised for cell size variability. Hence, normalised z values ranged from 0 (top of the cell) to 1 (bottom of the cell).

3. RESULTS AND DISCUSSION

A sample slice following preprocessing is shown in Figure 1A. The top-hat filter attenuates as expected all structures larger than the structuring element (Fig. 1B), in particular large domains present in the vacuole membrane. However, the thickness of the vacuole membrane is comparable to the diameter of the vesicles. Hence, the top-hat filter cannot discriminate between these two kinds of structures. On the contrary, the isotropy filter enhances spots at the expense of membranes (Fig. 1C), thus allowing the determination of a threshold to extract spots only (Fig. 1D).

Normalised grey level profiles along a segment passing through a spot and a vacuole membrane in these images are displayed in Figure 2. The first peak corresponds to a spot and the second one to a vacuole membrane. The ratio between spot and membrane peak values is 1.55 after average smoothing, 3.61 after top-hat filtering, and raises to 11.32 after isotropy filtering. These profiles confirm that, beyond top-hat filtering, the isotropy filter provides a large additional source of contrast between spots and other structures.

Cell contours were semi-automatically determined from user-provided cell markers (Fig. 1E) using an active contour approach (Fig. 1F). Three-dimensional graphical models of cell boundaries and spot positions were generated for interactive exploration of intra-cellular spot distributions (Fig. 3A).

The results of the automatic algorithm were compared to manually obtained results over 20 test cells. Though user-

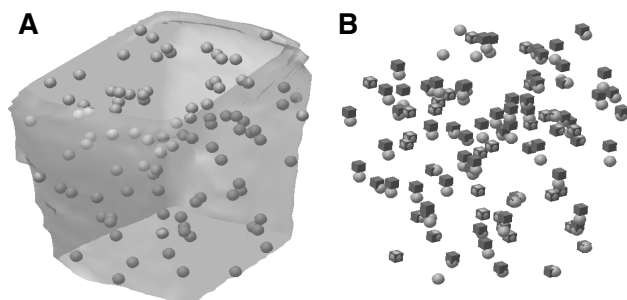


Fig. 3. Sample spot extraction result. (A) 3D model of a cell envelope (transparent surface) with barycenters of automatically detected spots (spheres). (B) Same as A with cell envelope removed and manually extracted spots added (cubes).

specified spot positions generally differed from the barycenters of automatically detected spots, the number of actual errors was very low. Figure 3B displays the test case that presented the highest error rates, with 5 false positives and 1 false negative over 98 automatically and 94 manually detected spots, respectively. Over the 20 test cells, 3.75% of the 694 manually recorded spots were not detected by the algorithm (false negatives). Among the 680 spots found by the algorithm, 1.76% did not correspond to manually detected spots (false positives). These low error rates demonstrate that the algorithm is very accurate at detecting spots.

The algorithm was applied to analyse the distribution of GFP-KOR1 vesicles in 46 cells under control conditions. The total number of detected spots was 1065. The number of spots per cell ranged from 2 to 96, with an average of 23.2 ± 22.4 . This large variability may be due to an inhomogeneous cell population and requires further examination. The distribution of spots normalised positions along the external/internal cell axis (z dimension) is shown in Figure 4. Globally, the density of GFP-KOR1 vesicles decreases with depth. Due to the high accuracy of the spot extraction method, it is unlikely that this decrease is due to detection errors. Wall synthesis in elongating cells such as epidermal root cells is not isotropic. The observed gradient of GFP-KOR1 vesicles could thus be correlated with the external/internal polarity of the cells. Lastly, the possibility that this effect is an artefact due to photobleaching cannot be completely ruled out.

4. CONCLUSION

We have shown that spots can be discriminated from other structures based on the isotropy of the spatial intensity distribution, as quantified from the spectrum of the second-order moment matrix. The proposed spot extraction filter has a high accuracy. The generalisation of the approach to any space dimension is straightforward.

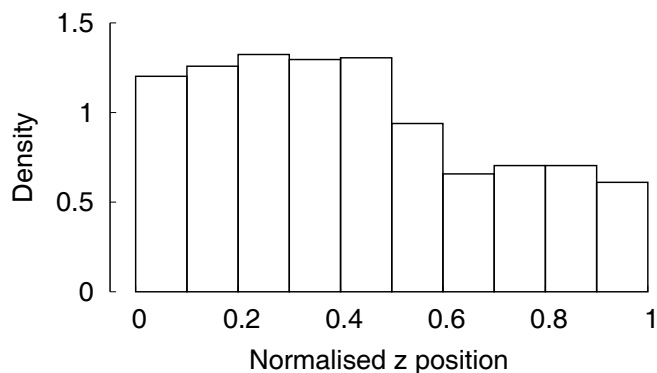


Fig. 4. Distribution of normalised z positions of GFP-KOR1 vesicles in control plant cells. The histogram has been normalised to sum to 1.

5. REFERENCES

- [1] P. Andrey and T. Boudier. Adaptive active contours (snakes) for the segmentation of complex structures in biological images. In *First ImageJ User & Developer Conference*, Luxemburg, 18–19 May 2006.
- [2] P. Andrey and Y. Maurin. *Free-D*: an integrated environment for three-dimensional reconstruction from serial sections. *J. Neurosci. Methods*, 145(1–2):233–244, 2005.
- [3] M. K. Cheezum, W. F. Walker, and W. H. Guilford. Quantitative comparison of algorithms for tracking single fluorescent particles. *Biophys. J.*, 81(4):2378–2388, 2001.
- [4] M. A. Estelle and C. Somerville. Auxin-resistant mutants of *Arabidopsis thaliana* with an altered morphology. *Mol. Gen. Genet.*, 206(2):200–206, 1987.
- [5] M. Gué, C. Messaoudi, J. S. Sun, and T. Boudier. Smart 3D-FISH: automation of distance analysis in nuclei of interphase cells by image processing. *Cytometry*, 67A(1):18–26, 2005.
- [6] J.-C. Olivo-Marin. Extraction of spots in biological images using multiscale products. *Patt. Recogn.*, 35(9):1989–1996, 2002.
- [7] S. Robert, A. Bichet, O. Grandjean, D. Kierzkowski, B. Satiat-Jeunemaître, S. Pelletier, M.-T. Hauser, H. Höfte, and S. Vernhettes. An *Arabidopsis* endo-1,4- β -D-glucanase involved in cellulose synthesis undergoes regulated intracellular cycling. *Plant Cell*, 17(12):3378–3389, 2005.
- [8] D. Thomann, D. R. Rines, P. K. Sorger, and G. Danuser. Automatic fluorescent tag detection in 3D with super-resolution: application to the analysis of chromosome movement. *J. Microsc.*, 208(1):49–64, 2002.